Ultrafast Kerr-induced all-optical wavelength conversion in silicon waveguides using 1.55 μm femtosecond pulses

R. Dekker, and A. Driessen.

Integrated Optical Micro Systems, Mesa+, University of Twente, P.O. Box 217, 7500 AE Enschede, The Netherlands.
R.Dekker@utwente.nl

T. Wahlbrink, and C. Moormann.

Advanced Microelectronic Center Aachen (AMICA), AMO GmbH, Huyskensweg 25, 52074 Aachen, Germany.

J. Niehusmann, and M. Först.

Institut für Halbleitertechnik, RWTH Aachen University, Sommerfeldstrasse 24, 52074 Aachen, Germany.

Abstract: The propagation of 300 femtosecond optical pulses in Silicon-on Insulator waveguides has been studied by means of a pump-probe set-up. The ultrafast pulses allowed the observation of large Kerr-induced red and blue shifts (9nm and 15nm, respectively) of the probe signal depending on the delay between pump (1554nm) and probe (1683nm) pulses. A numerical model taking into account the Kerr effect, Two Photon Absorption and Free Carrier Absorption is presented and provides good agreement with our experimental data and data in literature. A microring resonator based device is proposed that exploits the observed wavelength shift for sub-picosecond all-optical switching.

OCIS Codes: (130.4310) Integrated optics, nonlinear; (160.4330) Nonlinear optical materials; (190.2620) Frequency conversion; (230.1150) All-optical devices.

References and links

1. G. T. Reed, "Optical age of silicon," Nature **427**, 595-596 (2004).
2. V. Raghunathan, R. Claps, D. Dimitropoulos, and B. Jalali, "Parametric Raman wavelength conversion in scaled silicon waveguides," J. Lightwave Technol. **23**, 2094-2102 (2005).
3. A. Liu, H. Rong, M. Paniccia, O. Cohen, and D. Hak, "Net optical gain in a low loss silicon-on-insulator waveguide by stimulated Raman scattering," Opt. Express **12**, 4261-4268 (2004).
4. Q. Xu, V. R. Almeida, and M. Lipson, "Time-resolved study of Raman gain in highly confined silicon-on-insulator waveguides," Opt. Express **12**, 4437-4442 (2004).
5. T. K. Liang, H. K. Tsang, I. E. Day, J. Drake, A. P. Knights, and M. Asghari, "Silicon waveguide two-photon absorption detector at 1.5μm wavelength for autocorrelation measurements," Appl. Phys. Lett. **84**, 2745-2747 (2002).
6. O. Boyraz, T. Indukuri, and B. Jalali, "Self-phase-modulation induced spectral broadening in silicon waveguides," Opt. Express **12**, 829-834 (2004).
7. R. Dekker, E. J. Klein, J. Niehusmann, M. Först, F. Ondracek, J. Ctyroky, N. Usechak, and A. Driessen, "Self phase modulation and stimulated Raman scattering due to high power femtosecond pulse propagation in silicon-on-insulator waveguides," presented at the Symposium IEEE/LEOS Benelux Chapter, Mons, Belgium, (2005).
8. E. Dulkeith, Y. A. Vlasov, X. Chen, N. C. Panoiu, R. M. Osgood Jr., "Self-phase-modulation in submicron silicon-on-insulator photonic wires," Opt. Express **14**, 5524-5534, (2006).
9. O. Boyraz, P. Koonath, V. Raghunathan, and B. Jalali, "All optical switching and continuum generation in silicon waveguides," Opt. Express **12**, 4094-4102 (2004).

#71803 - $15.00 USD Received 9 June 2006; revised 21 August 2006; accepted 24 August 2006

10. H. Fukuda, K. Yamada, T. Shoji, M. Takahashi, T. Tsuchizawa, T. Watanabe, J. Takahashi, and S. Itabashi, "Four-wave mixing in silicon wire waveguides," Opt. Express **13**, 4629-4637 (2005).
11. M. Dinu, F. Quochi, and H. Garcia, "Third-order nonlinearities in silicon at telecom wavelengths," Appl. Phys. Lett. **82**, 2954-2956 (2003).
12. T. K. Liang and H. K. Tsang, "Nonlinear absorption and Raman scattering in silicon-on-insulator optical waveguides," IEEE J. Sel. Top. Quantum Electron. **10**, 1149-1153 (2004).
13. H. Rong, A. Liu, R. Nicolaescu, M. Paniccia, O. Cohen, and D. Hak, "Raman gain and nonlinear optical absorption measurements in a low-loss silicon waveguide," Appl. Phys. Lett. **85**, 2196-2198 (2004).
14. R. Claps, V. Raghunathan, D. Dimitropoulos, and B. Jalali, "Influence of nonlinear absorption on Raman amplification in Silicon waveguides," Opt. Express **12**, 2774-2780 (2004).
15. R. A. Soref and B. R. Bennett, "Electrooptical effects in silicon," IEEE J. Quantum Electron. **QE-23**, 123-129 (1987).
16. J. I. Dadap, R. L. Espinola, R. M. Osgood Jr., S. J. McNab, and Y. A. Vlasov, "Spontaneous Raman scattering in ultrasmall silicon waveguides," Opt. Lett. **29**, 2755-2757 (2004).
17. Y. Liu and H. K. Tsang, "Nonlinear absorption and Raman gain in helium-ion-implanted silicon waveguides," Opt. Lett. **31**, 1714-1716, (2006).
18. X. Chen, N. C. Panoiu, and R. M. Osgood Jr., "Theory of Raman-mediated pulsed amplification in silicon-wire waveguides," IEEE J. Quantum Electron. **42**, 160-170 (2006).
19. FieldDesigner, www.phoenixbv.com.
20. E. D. Palik, "Handbook of Optical Constants of Solids," (Academic Press, 1998).
21. Q. Xu, V. R. Almeida, and M. Lipson, "Demonstration of high Raman gain in a submicrometer-size silicon-on-insulator waveguide," Opt. Lett. **30**, 35-37 (2005).
22. D. J. W. Klunder, F. S. Tan, T. van der Veen, H. F. Bulthuis, G. Sengo, B. Docter, H. J. W. M. Hoekstra, and A. Driessen, "Experimental and numerical study of SiON Microresonators with air and polymer cladding," J. Lightwave Technol. **21**, 1099-1110 (2003).
23. D. H. Geuzebroek, E. J. Klein, H. Kelderman, N. Baker, and A. Driessen, "Compact wavelength-selective switch for Gigabit Filtering in Access Networks," IEEE Photon. Technol. Lett. **17**, 336-338, (2005).
24. V.R. Almeida, and M. Lipson, "Optical bistability on a silicon chip," Opt. Lett. **29**, 2387-2389, (2004).

Introduction

Silicon photonics is receiving increasingly attention, especially because of its potential for integration with microelectronics [1]. In recent years many new types of nonlinear optical phenomena have been investigated in silicon-based nanophotonic devices. Substantial progress has been achieved, e.g., in the field of Raman amplification, in both continuous-wave [2] and pulsed pump-probe [3, 4] experiments. Further nonlinear effects like two-photon absorption (TPA) [5], self-phase modulation (SPM) [6-8], cross-phase modulation (XPM) and continuum generation [9], four-wave mixing (FWM) [10] and the Kerr effect [11] have also been successfully demonstrated and thoroughly investigated – typically on time scales ranging from the picosecond to the nanosecond regime. In detail, a careful analysis of self-phase modulation in submicron silicon waveguides was recently presented by Dulkeith *et al.* [8]. They investigated the spectral broadening of picosecond pulses as a function of power and wavelength upon waveguide propagation. Beyond this study of self-phase modulation, Boyraz *et al.* [9] reported all-optical switching based on constructive and destructive interference exploiting cross phase modulation of a CW signal in a Mach Zehnder interferometer. Although the optical pump beam produced sub-picosecond pulses, the off-switching time in their experiments was limited to ~7ns, as a result of the free carrier lifetime. Xu *et al.* [4] reported a 1.6nm wavelength shift of a CW probe signal caused by cross phase modulation using 3.5ps pump pulses. They exploited the wavelength shift to demonstrate all-optical switching by using a tunable grating filter at the output of the waveguide.

In this paper, we present a theoretical and experimental analysis of cross phase modulation induced wavelength conversion in Silicon-on-Insulator (SOI) waveguides on the sub-picosecond timescale. The duration of both the pump and the probe pulses was 300fs. To our best knowledge, this is the first time that large XPM induced wavelength shifts of 15nm in submicron sized SOI waveguides taking place on a sub-picosecond timescale are being reported. We used femtosecond pulses for this investigation since these typically offer higher peak intensities compared to nanosecond and picosecond pulses, and therefore are very attractive for nonlinear operation. In our case, ultrafast Kerr-induced refractive index changes

#71803 - $15.00 USD Received 9 June 2006; revised 21 August 2006; accepted 24 August 2006

are predominantly responsible for a temporal variation in phase, causing a wavelength shift of the probe signal. This shift is proportional to the first derivative with respect to time of the pulse envelope, being 1 to 2 orders of magnitude larger than the up to now reported experiments with pulses in the ps regime. The XPM induced frequency shift is not limited in speed by the free carrier lifetime. Instead, the frequency conversion takes place mainly during the leading and trailing edges of the 300fs pulses, *i.e.* in a sub-picosecond timeframe.

The temporal shape of the pump pulses is investigated using a theoretical model including TPA and free carrier absorption (FCA). The contributions of both the Kerr nonlinearity and the free carrier dispersion caused by the pump pulses are used to explain the experimentally observed wavelength shift of the probe signal. Based on a simple model, numerical results of femtosecond, picosecond and nanosecond pulse propagation in SOI waveguides is presented and compared to recent experimental data from ourselves and literature. In addition, the importance of waveguide dispersion on the conversion efficiency using sub-picosecond pulses will be discussed. Finally, a novel sub-picosecond all-optical switching scheme based on the observed wavelength shift and a passive microring resonator is proposed.

Theory

At the SOI waveguide input, the envelope of the pump pulses in our experiments can be described by a Gaussian:

$$I(t,0) = I_{\max}.e^{-0.5.\left(\frac{|t-t_0|}{\delta}\right)^2} \tag{1}$$

where I_{max} is the peak intensity in W/cm^2 and δ is the standard deviation that is related to the full width at half maximum duration (FWHM) of the pulse, which is defined as $FWHM = 2.3548 \cdot \delta$ (~300fs in our experiments). During propagation along the waveguide the intensity of the pulse $I(t,z)$ decreases due to several loss mechanisms, mainly linear absorption and scattering, two-photon absorption (TPA) and free carrier absorption (FCA). Therefore, the change of pump intensity along the waveguide may be described as [3]:

$$\frac{dI(t,z)}{dz} = -\alpha I(t,z) - \beta I^2(t,z) - \sigma N(t,z) I(t,z) \tag{2}$$

where α is the linear absorption, β is the two photon absorption coefficient (ranging from $0.5 \cdot 10^{-9}$ to $0.9 \cdot 10^{-9}$cm/W [3, 11-14]), $N(t,z)$ is the free carrier density in cm^{-3} and σ is the free carrier absorption cross section. According to Soref *et al.* [15] $\sigma = 1.45 \cdot 10^{-17} \cdot (\lambda/1.55)$ cm^2, where λ is the wavelength in micron. As the losses are a function of time via the free carrier density $N(t,z)$ and the light intensity $I(t,z)$, the original Gaussian pulse shape is not conserved during propagation along the waveguide. The time dependence of the free carrier density in the silicon waveguide can be written in terms of electron-hole pair generation and recombination [3]:

$$\frac{dN(t,z)}{dt} = \frac{\beta}{2h\nu} I^2(t,z) - \frac{N(t,z)}{\tau} \tag{3}$$

where $h\nu$ is the photon energy and τ is the free carrier lifetime. The latter depends strongly on the method used for fabrication of the wafer [9] and the waveguide geometry [14]. The free carrier diffusion away from the waveguide mode area and recombination at the waveguide surface are the dominant effective lifetime reducing mechanisms in SOI waveguides. The effective free carrier lifetime in our waveguides is likely to be in the order of a few ns (see Dadap *et al.* [16]). Although it is hard to compare the lifetimes of different fabrication methods, the results of our model, i.e. the propagation characteristics of 300fs pulses, do not change noticeably, when carrier lifetimes are varied over the range from 100ps to 10ns. The propagation of sub picosecond pulses does not change until the lifetime is decreased to tens of picoseconds. A free carrier lifetime reduction from 100ns to 1.9ns has recently been

#71803 - $15.00 USD Received 9 June 2006; revised 21 August 2006; accepted 24 August 2006

demonstrated using helium implantation of silicon waveguides [17]. In this case the recombination does not mainly occur at the waveguide interfaces, but primarily at recombination centers introduced inside the waveguide. Since our waveguides did not experience any implantation damage, we assumed the lifetime to be larger than 1 ns.

The set of coupled differential equations, Eq. (2) and (3) have been solved numerically to get insight about the physical effects in our pump-probe experiments. The results are presented in Table 1 for several pulse durations.

Short pulses propagating along the silicon waveguide do not only experience losses, but also refractive index changes caused by the Kerr effect and the generated free carriers. The Kerr induced refractive index change is described by:

$$\Delta n_{Kerr}(t,z) = n_2 . I(t,z) \tag{4}$$

where n_2 ranges from $4 \cdot 10^{-14}$ to $9 \cdot 10^{-14}$ cm^2/W [10, 11]. We have used $n_2 = 4 \cdot 10^{-14}$ cm^2/W in our simulations. The free carrier induced refractive index change has an opposite sign and can be described by the well-known accurate empirical relation presented by Soref *et al.* [15]:

$$\Delta n_{FC}(t,z) = -(8.8 \cdot 10^{-22} N_e(t,z) + 8.5 \cdot 10^{-18} N_h(t,z)^{0.8}) \tag{5}$$

where subscripts *e* and *h* denote electrons and holes, respectively. Since the number of electrons and holes created by TPA are equal, $N_e(t,z)$ and $N_h(t,z)$ can be replaced by $N(t,z)$ in units of cm^{-3} in Eq. (5).

Next, consider a pump-probe experiment where the delay time between the pulses is such that the probe signal has a temporal overlap with the pump signal on either the rising or trailing edge. In this case, the probe signal will experience a time dependent phase shift $\Delta\phi(t,z)$ which is caused by the temporal change in the pump pulse induced index changes [4]:

$$\Delta\phi(t,z) = \frac{2\pi L_{\text{int}}}{\lambda}\left[\Delta n_{Kerr}(t,z) + \Delta n_{FC}(t,z)\right] \tag{6}$$

Here L_{int} is the interaction length, *i.e.* the length over which the pump and probe pulses feel each others presence. This temporal variation in phase will result in a frequency shift of the probe pulses:

$$\Delta\omega(t,z) = -\frac{d}{dt}\Delta\phi(t,z) \tag{7}$$

resulting in a shifted center wavelength of the probe pulses:

$$\lambda_s = \frac{\lambda_0}{1 - \frac{L_{\text{int}}}{c} \cdot \frac{\Delta n(t,z)}{dt}} \tag{8}$$

where λ_s is the center wavelength of the frequency converted probe pulse, λ_0 the center wavelength of the original probe spectrum and c is the speed of light in vacuum.

Experimental setup

Figure 1 shows a schematic representation of our experimental setup. Both the pump (1554nm) and probe (1683nm) pulses with a FWHM pulse duration of 300fs are delivered by an optical parametric oscillator (OPO). With a repetition rate of 80MHz the time between the pulses is 12.5ns. This is in the same order of magnitude as the free carrier lifetime, but in case of sub-picosecond pulses this won't affect the temporal characteristics of the pulses, as will be discussed in the next paragraph. The time delay between pump and probe pulses is controlled with a free-space optical delay line (ODL) with 6.6 femtosecond accuracy. Both beams are combined using a beam splitter (BS) and coupled into a 10cm piece of polarization

#71803 - $15.00 USD Received 9 June 2006; revised 21 August 2006; accepted 24 August 2006

maintaining fiber (PMF) using a microscope objective (MO), while their shapes are being modified by optical beam formers (OBF) in order to optimize the fiber coupling efficiency. The output of the PMF (30mW average power for the pump and 3mW for the probe) is used to facilitate the simultaneous coupling of the TM polarized pulses into our SOI waveguides that have a 450nm×300nm (w×h) cross section (by design) and a length *L* of 7mm. No spectral broadening due to the fiber nonlinearities has been observed at the output of the fiber, prior to entering the SOI waveguide. After propagation through the SOI waveguide the transmitted pulses are coupled out using a single mode fiber, which is attached to an optical spectrum analyzer (OSA). By this means, both intensity and spectral characteristics of the transmitted pump and probe pulses can be detected simultaneously. Folding mirrors (FM) are used to tap the pump and probe signals in front of the waveguide for power level detection using an optical detector (OD). The pump intensity can be controlled using a neutral density filter (NDF). A nonlinear crystal (BBO) is used to determine the zero time delay by detecting the sum frequency of pump and probe (808nm) with the OSA.

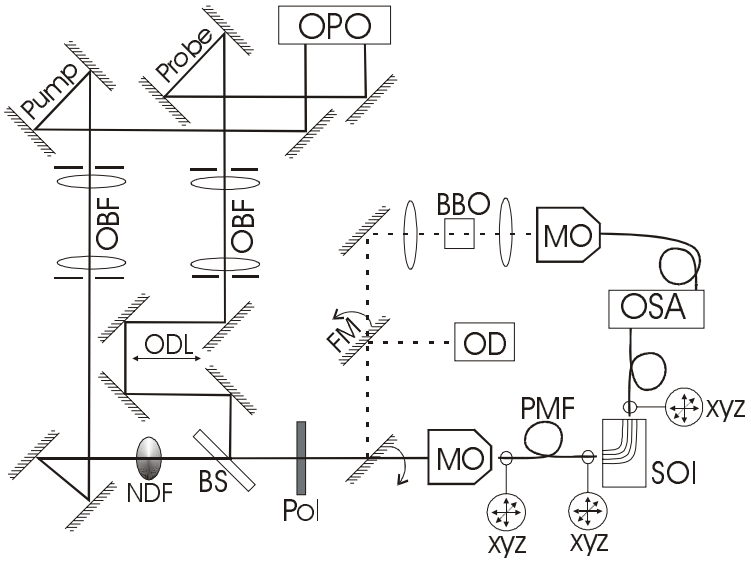

Fig. 1. Schematic representation of the pump-probe setup.

Experimental results

The probe transmission integrated over the pulse spectrum as function of delay time is shown in Fig. 2. Here a negative delay time means that the probe pulses are running ahead of the pump pulses, or are overlapping with the leading edge of the pump pulse. Dispersion management is crucial in case of sub-ps pulses as will be discussed later. Therefore, the waveguide width that strongly influences the waveguide dispersion has been chosen such that the walkoff length [18], *i.e.* the distance over which the pump and probe pulses pass through each other's envelope, was larger than the waveguide length *L*.

#71803 - $15.00 USD Received 9 June 2006; revised 21 August 2006; accepted 24 August 2006

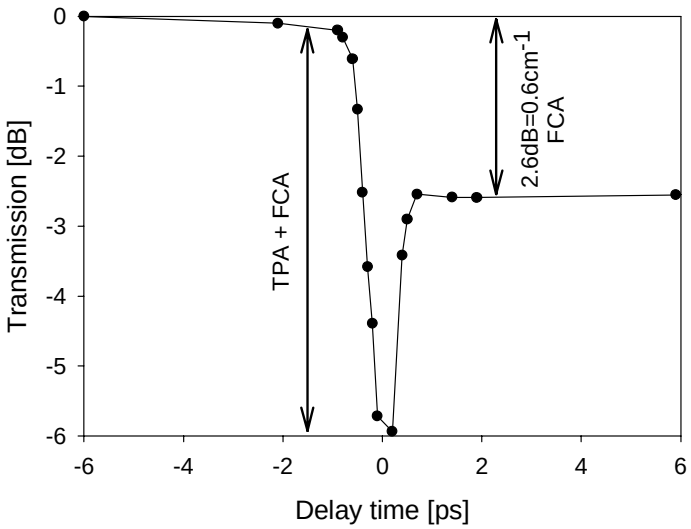

Fig. 2. Probe signal transmission as function of delay time.

The 2.6dB loss for positive time delays is solely caused by the TPA induced FCA. By dividing the FCA by the free carrier absorption cross section σ, the FC concentration in the waveguide was determined to be $N \approx 4 \cdot 10^{16} cm^{-3}$. For the generation of this free carrier density, the average power inside the waveguide was estimated to be ~500μW which corresponds to peak intensities in the order of $15 GW/cm^2$ and a pulse energy of only 7.5pJ. The simulated pump pulse envelopes $I(t,z)$, the corresponding free carrier densities $N(t,z)$, both as function of propagation distance, and the Kerr and FC induced refractive index changes Δn_{Kerr} and Δn_{FC} are listed in Table 1. A comparison is made with the 3.5ps and 17ns pulse experiments in SOI waveguides from Xu *et al.* [4] and Liu *et al.* [3], respectively, to illustrate the differences in the cross-phase modulation characteristics for laser pulses of distinct pulse length regimes.

From the graphs shown in Table 1 several conclusions can be drawn. In case of sub-picosecond pump pulses the loss mechanism is dominated by TPA, whereas in the nanosecond pulse regime the cumulative effect of FCA comes into play together with TPA. In the latter case the losses are dominated by FCA resulting in a dramatic disturbance of the Gaussian pulse shape. Besides the pulse shapes, Table 1 also displays the contributions of the Kerr nonlinearities [Eq. (4)] and the free carriers [Eq. (5)] to the total refractive index change. In the case of 300fs pulses used in our experiment, it can be seen that the total refractive index change is determined chiefly by the Kerr nonlinearities, whereas the Kerr and FC effect are balanced in the ps case and the Kerr contribution can be neglected in the ns regime. In the last row of Table 1 an estimate is given of the wavelength shifts that can be expected in fs, ps and ns pump-probe experiments. The reason for the large difference in wavelength shift between pulses in the femtosecond regime and the work of Xu *et al.* [4] in the picosecond regime is solely a pulse duration effect. Although the peak intensities are both in the order of $15 GW/cm^2$, the Kerr-induced temporal phase change, which is proportional to the time derivative of the pump pulse, of the 300fs pulses is much more abrupt, and therefore expected to result in a larger XPM induced frequency shift, according to Eq. (7).

The experimental and simulated probe wavelength shifts caused by the 300fs pump induced temporal refractive index change are plotted in Fig. 3. The center wavelengths of the shifted probe pulses have been determined by fitting a symmetrical Gaussian spectral shape and taking the center of the fitted spectrum. A red- and blue-shift for the transmitted probe pulses for negative and positive time delays, respectively, is clearly observed in both the experimental and simulation data. Note the asymmetry in the wavelength shift on the trailing and falling edges of the pulse, i.e. a red-shift of about 10nm but a stronger blue-shift of about

#71803 - $15.00 USD Received 9 June 2006; revised 21 August 2006; accepted 24 August 2006

Table 1. Temporal characteristics of pulse propagation in SOI waveguides for different pulse durations. Simulations of the pulse intensities, free carrier densities and refractive index change as function of time are shown for 300fs, 3.5ps and 17ns experiments, respectively. The last row shows the XPM induced wavelength shift of the probe signal.

Par.	**300 femtoseconds**	**3.5 picoseconds**	**17 nanoseconds**
Ref	This work	[4]	[3]
$w \times h$	450×300nm	450×250nm	1520nm×1450nm (rib)
A_{eff}	~0.15μm^2	~0.14μm^2	~1.5μm^2
L	7mm	7mm	48mm
τ	5ns	5ns	25ns
I_{max}	~15GW/cm^2	~15GW/cm^2	~50MW/cm^2
F_{rep}	80MHz	76.8MHz	10KHz
λ_p	1554nm	1589.5nm	1545nm
λ_s	1683nm	1731.5nm	1680nm
I(t)	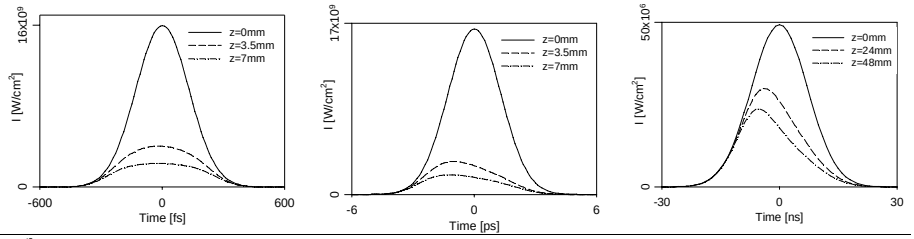		
N(t)	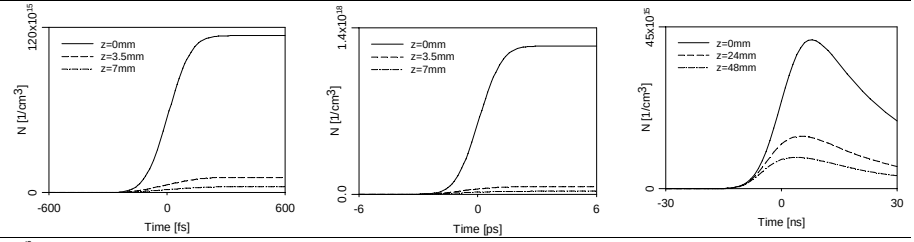		
Δn z=L	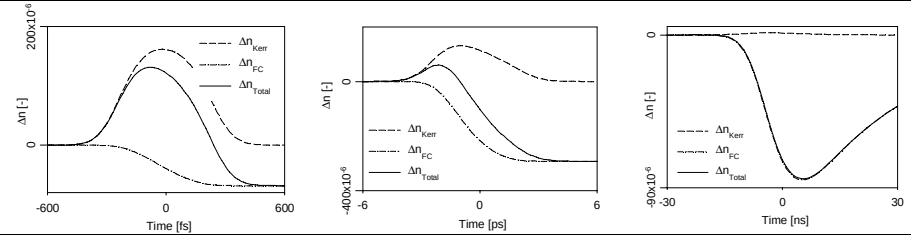		
λ_{probe}	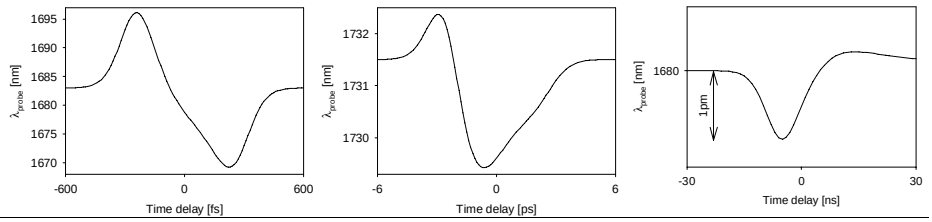		

#71803 - $15.00 USD Received 9 June 2006; revised 21 August 2006; accepted 24 August 2006

15nm. Contributions of free carriers to the refractive index change are of negative sign and therefore support a blue-shift of the center wavelength over the entire pulse where the free carrier concentration changes in time. There is good agreement between the experimental and simulation data. The discrepancy in the magnitude of the red shift, however, might be caused by the dispersion properties of the waveguides, which are not taken into account in our model. Another cause may be due to some uncertainty in the determination of the center wavelength or the resolution in the delay time. The experimental determination of the center wavelength was difficult as the waveguide output signal was very weak at positive delay times because of the TPA and FCA losses (see Fig. 2). As mentioned earlier, the magnitude of the observed red and blue-shifts in our experiments are larger as those observed in the work of Xu *et al.* [4], who reported a 1.6nm blue-shift using ps-pulses. The latter value is also predicted by our model due to the free carrier contribution as can be seen in the last row of Table 1. Furthermore, it can be concluded from Table 1 that a ~1nm Kerr induced redshift can be achieved when the probe pulse is overlapping with the leading edge of a ps-pump pulse. In case of nanosecond pulses, where the FC dispersion dominates over the Kerr effect, only a 1 picometer blue shift takes place at negative delay times and an even smaller red shift at positive delay times, respectively.

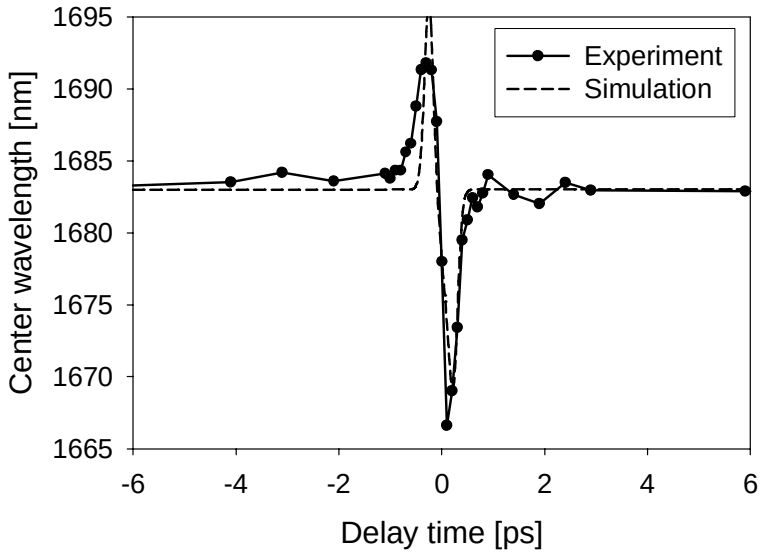

Fig. 3. Center wavelength of the probe signal as function of delay time.

Waveguide dispersion

In case the SOI waveguide dimensions are in the submicron range, the geometry induced waveguide dispersion will dominate the material dispersion [18]. The characteristic walkoff length L_w represents the distance over which the pump and probe pulses pass through each other's envelope [18]:

$$L_w(\lambda) = T_0 \Big/ \left| \beta_{1p}(\lambda) - \beta_{1s}(\lambda) \right| \tag{9}$$

#71803 - $15.00 USD Received 9 June 2006; revised 21 August 2006; accepted 24 August 2006

where T_0 is the width of the pulse (at 1/e intensity), and $\beta_{1p}(\lambda)$ and $\beta_{1s}(\lambda)$ are the first order dispersion coefficients of the pump and probe wavelengths, respectively. In Fig. 4 the first order dispersion coefficients, usually referred to as the reciprocal group velocity, and walkoff lengths between the 1554nm pump and 1683nm probe pulses are plotted for a SOI waveguide with a height of 300nm and the width as varying parameter. The effective mode indices needed for the determination of the dispersion coefficients were obtained with the aid of a full vectorial finite difference based mode solver [19] taking the silicon material dispersion into account [20]. It can be seen that the waveguide width is a critical parameter that strongly affects the pump-probe interaction and therefore the maximum attainable wavelength conversion as the conversion efficiency increases with L_w. In case of Raman amplification the dispersion is less critical, since the lifetime of the optical phonons in silicon is in the order of 3ps [21] facilitating a temporal overlap of the phonon lifetimes and the probe pulses up to delay times of a few ps.

Since the walkoff length scales linearly with the pulse length [Eq. (9)], it can be concluded that the interaction length can easily be increased by increasing the pulse lengths. However, at longer pulse lengths the pulse envelope is less steep resulting in weaker wavelength conversion. Therefore we believe that the observed large wavelength shifts in SOI can only be achieved with sub-picosecond pulses, combined with precise control of the waveguide dispersion.

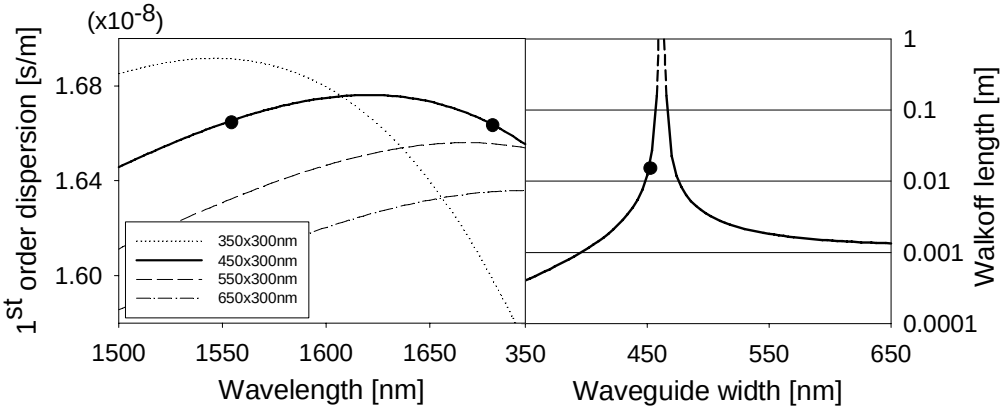

Fig. 4. Left: first order dispersion as a function of wavelength. Pump and probe wavelengths are marked with black dots. Right: walkoff length as function of waveguide width. The waveguide width of the waveguide used in the experiments is marked with a black dot.

Ultrafast all-optical switching

Sub-picosecond all optical switching can be achieved by the investigated Kerr-induced wavelength conversion in case the SOI waveguide is combined with a SOI microring resonator filter. Integrated optical microring resonators are known for their compact size and favorable filter shapes and have been studied extensively in both single [22] and multiple microring resonator configurations [23]. In Fig. 5 a typical microring resonator filter response is shown, calculated using the transfer functions of a 4 port microring resonator. The total wavelength conversion that has been achieved with our sub-ps pump-probe experiment is ±10nm, which is in the order of the free spectral range (FSR) of a ring resonator with a radius of 10μm. This means that the probe signal can be tuned over the full FSR of the ring by adjusting the time delay. This is illustrated in Fig. 5, where the center wavelength of the shifted probe signal is plotted above the spectral response of a microring resonator. The power needed in the pump control pulse to achieve the needed wavelength shift is in the order of 7.5pJ. The nonlinear wavelength conversion takes place in the input port waveguide, while the wavelength shifted probe signal is being filtered with the passive microring resonator.

#71803 - $15.00 USD Received 9 June 2006; revised 21 August 2006; accepted 24 August 2006

The novelty of this all-optical switching scheme is that the port waveguide is the active nonlinear component, whereas the microring resonator is acting as a passive wavelength dependent space switch. Since the wavelength conversion is determined by the time derivative of the refractive index change, the switching time of such a switch is directly related to the width of the pump pulse [4], which is in the order of 300fs. This is in contrast to the all-optical switching mechanisms that rely on the FC dispersion, where the switching speed is limited by the FC lifetime which is typically in the order of nanoseconds. An alternative switching scheme is proposed by others where the microring resonator acts as the nonlinear element [24]. The field buildup in the resonant structure will induce either a thermal, Kerr or free carrier induced refractive index change. The refractive index change will in turn shift the resonance spectrum (and not the probe signal) which is used to switch a signal. However, in order to sufficiently benefit from the field buildup in a microring resonator, high Q resonators are needed that typically show a slow response and are bistable. In our proposed case, low Q passive microring resonators having short loading and unloading times can be used, because the large pump induced wavelength shift of the probe signal takes place in the non-resonant input port waveguide. The loading and unloading time of a resonator with a quality factor of ~1000 (finesse~10) is in the order of a few ps, which is one order of magnitude longer than the sub-ps timeframe in which the wavelength conversion takes place. However, in the case of an optical time division multiplexing scheme, these loading and unloading times won't form a bottleneck for bitrates below 100 Gbit/s.

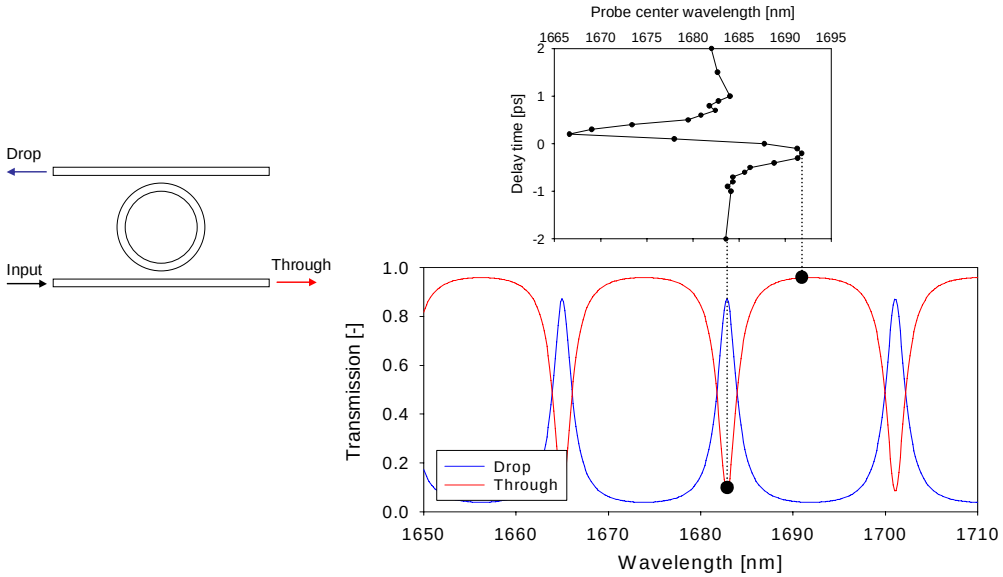

Fig. 5. Schematic representation of an all-optical switching scheme consisting of an active SOI waveguide channel for the wavelength conversion and a passive SOI ring resonator for the wavelength dependent space switching. The experimentally observed wavelength shift as function of delay time is projected on top of the theoretical spectral response of a microring resonator to illustrate the working principle of this all-optical switching scheme.

Conclusion

We have shown that both larger 10nm blue and red shifts of signal light are feasible in SOI waveguides by exploiting the ultrafast Kerr-induced refractive index changes induced by 300fs laser pulses. The use of a simple model reveals that the temporal refractive index changes are mainly caused by the instantaneous Kerr effect and thus both the wavelength up- and down-conversion takes place in a sub-picosecond timeframe. Experimental results have been compared with simulation data and show good agreement. Furthermore, we have shown the importance of waveguide dispersion on the cross-phase modulation conversion efficiency

#71803 - $15.00 USD Received 9 June 2006; revised 21 August 2006; accepted 24 August 2006

in case of sub-picosecond pump-probe experiments. The results open the way to sub-picosecond all-optical switching using SOI microring resonators or waveguide gratings.

Acknowledgments

R. Dekker and A. Driessen would like to thank Freeband Impulse technology program of the Ministry of Economic Affairs of the Netherlands. All authors would like to acknowledge the European Network of Excellence on Photonic Integrated Components and Circuits (ePIXnet FAA5/WP11).

#71803 - $15.00 USD Received 9 June 2006; revised 21 August 2006; accepted 24 August 2006